An Integrated Workflow for Urban Tree DBH Estimation from Handheld Mobile Laser Scanning (HMLS) Data

George-Catalin Males[1], Valeria-Ersilia Oniga[1,2], Iosif Lavric[1], Norbert Pfeifer[3], Markus Hollaus[3]

[1] Department of Topography and Cadastre, Faculty of Geodesy, Technical University of Civil Engineering Bucharest, Bucharest, Romania – (catalin.males, iosif.lavric)@phd.utcb.ro

[2] Department of Land Surveying and Cadastre, Technical University „Gheorghe Asachi" of Iasi, D. Mangeron Street, Iasi, Romania – valeria-ersilia.oniga@academic.tuiasi.ro

[3] Department of Geodesy and Geoinformation, Technische Universität Wien, Karlsplatz 13, 1040 Vienna, Austria – (norbert.pfeifer, markus.hollaus)@geo.tuwien.ac.at

Keywords: HMLS, GoSLAM, FJD Trion S1, DBH, urban park.

Abstract

The stem diameter is a fundamental parameter for assessing woody vegetation growth and quantifying ecological and economic benefits such as biomass production, carbon sequestration, and urban ecosystem services. Recent advances in handheld mobile laser scanning (HMLS) enable efficient acquisition of high-density point clouds for deriving tree structural attributes in complex urban environments. This study presents an automated workflow for tree detection and diameter at breast height (DBH) estimation in an urban park using two HMLS systems: the GoSLAM RS100i and the FJD Trion S1. The analysis evaluates the influence of point cloud density and subsampling resolution on detection performance and DBH accuracy. Reference measurements for 69 trees were collected using a forestry caliper and total station, while HMLS datasets were georeferenced with RTK-GNSS observations. The workflow included point cloud filtering, terrain modelling, stem extraction, and DBH estimation through cylindrical fitting. Detection performance differed between systems and was strongly affected by point density. The GoSLAM RS100i showed a decline in correctly detected trees from 97.1% at 2 cm spacing to 53.6% at 4 cm, whereas the FJD Trion S1 maintained stable detection rates of approximately 87% across all spacings, likely due to its higher point density. DBH estimation accuracy was comparable for both systems, with RMSE values of 3.3–3.6 cm for filtered datasets and up to 4.9 cm when all detections were included. A systematic positive bias of 1.7–2.5 cm was observed. Results demonstrate that HMLS systems provide reliable DBH estimates for efficient urban tree inventory applications.

1. INTRODUCTION

The use of two-dimensional (2D) and three-dimensional (3D) geospatial data is fundamental for the effective monitoring of urban vegetation. Among urban green elements, trees are particularly important, as they provide a wide range of ecological, environmental, and social benefits. For instance, urban trees help reduce ambient temperatures through shading and evapotranspiration, while also improving air quality by absorbing gaseous pollutants and trapping airborne particles on leaf and bark surfaces (Gillner et al., 2015; Jayasooriya et al., 2017). Moreover, urban vegetation mitigates stormwater runoff by capturing and retaining rainwater, thereby decreasing the risk of flood-related damage (Liu et al., 2025).

An urban tree inventory represents a systematic process for collecting detailed information on individual trees within urban environments, including those along streets, in parks, and across other public or private spaces. The inventory typically records key biophysical and structural attributes such as species, georeferenced location, diameter at breast height (DBH), tree height, crown dimensions, health condition, and maintenance requirements. This information forms the basis for understanding urban vegetation and provides essential information for local authorities in identifying and monitoring dynamic processes, as well as supporting urban planning and management activities. DBH is one of the most important parameters required for urban tree inventory.

Various technologies have been developed to estimate stem diameter, ranging from traditional field-based measurements to advanced remote sensing techniques. The most conventional approach involves manual calliper or diameter tape measurements at breast height (1.3 m above the terrain) (Binot et al., 1995), which provide high accuracy but are labor-intensive and limited in spatial coverage (Piermattei et al., 2019). Advances in terrestrial laser scanning (TLS) (Koreň et al., 2017; Liang et al., 2016, 2018) and mobile laser scanning (MLS) (Oveland et al., 2017) have enabled detailed three-dimensional (3D) reconstructions of tree stems, allowing automated or semi-automated DBH extraction with millimetric precision. Airborne laser scanning (ALS) and unmanned aerial vehicle (UAV)-based LiDAR systems (ULS) (Mandlburger et al., 2015) extend this capability to larger forested areas, though typically with reduced accuracy at the individual tree level due to lower point densities on the stems and near the ground. More recently, handheld mobile laser scanning (HMLS) employing high-precision SLAM algorithms for automatic point cloud registration without GNSS signals (Liu et al., 2021; Fan et al., 2021; Zhou et al., 2019) and structure-from-motion (SfM) photogrammetry (Piermattei et al., 2019; He et al., 2025) have emerged as flexible alternatives, offering a balance between accuracy, portability, and acquisition efficiency. Studies comparing HMLS and TLS show that HMLS offers higher efficiency in forest parameter acquisition, particularly for DBH, while TLS provides more detailed canopy information (e.g. Liu et al., 2021).

DBH estimation from HMLS point clouds can achieve high accuracy, with some studies reporting root mean square error (RMSE) as low as ~ 20 mm. Accuracy is influenced by factors like point cloud density, scanner precision (range and angular accuracy), number of scans, and processing algorithms. Point cloud density is a significant factor, as it impacts the number of points available for fitting a circle to the trunk's cross-section.

The integration of these technologies with machine learning and point cloud segmentation algorithms further enhances the automation and reliability of DBH estimation across diverse forest environments.

Our study introduces an integrated workflow for automatic tree detection and diameter at breast height (DBH) estimation in an urban park environment, evaluated using two HMLS systems, the GoSLAM RS100i and the FJD Trion S1. Particular emphasis is placed on the influence of point cloud density and subsampling resolution on detection performance and estimation accuracy. The implemented workflow integrates key modules of the OPALS software (Pfeifer et al., 2014), including the DBH module used for stem detection and diameter estimation. In addition to DBH accuracy, the study analyses detection completeness (precision and recall) and the robustness of the workflow under varying data densities.

2. MATERIAL AND METHOD

2.1 Processing workflow for individual tree detection and DBH estimation from HMLS data

The processing workflow used for stem detection and DBH estimation from HMLS point clouds is illustrated in Figure 1 and consists of four main stages. (1) Data acquisition, using two HMLS systems (GoSLAM RS100i and FJD Trion S1), with the latter configured in backpack mode and integrated with a GNSS receiver, including the marking and measurement of ground control points (GCPs) and the acquisition of reference data for DBH estimation and tree positions; (2) Data pre-processing, comprising HMLS point cloud registration, georeferencing, filtering, and subsampling; (3) Stem point extraction, including DTM and DSM needed for point cloud normalization and tree height extraction; (4) DBH estimation.

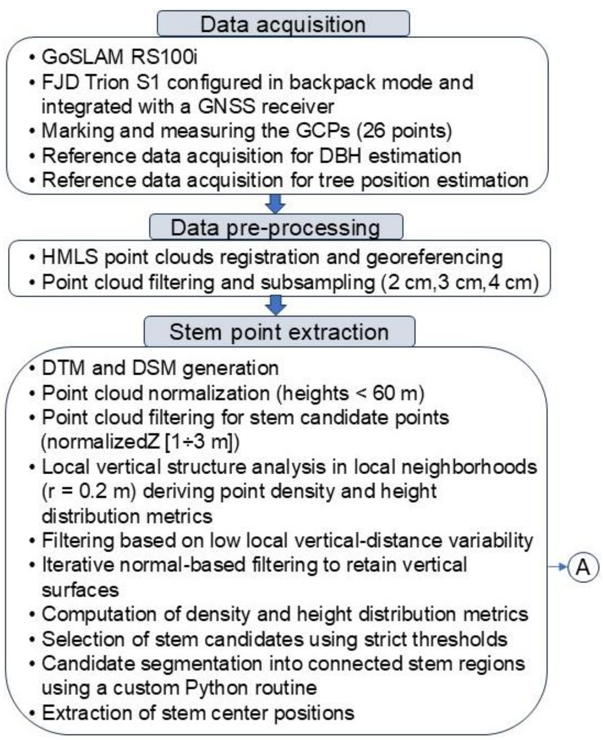

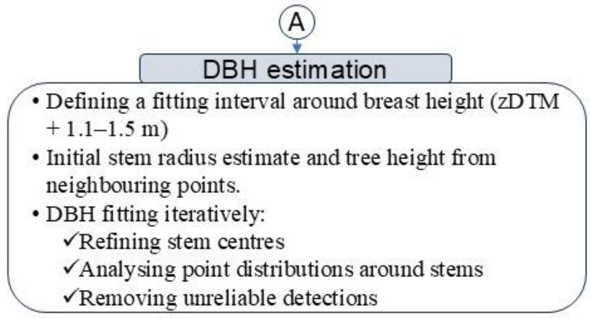

Figure 1: The workflow for tree stem detection and DBH estimation from HMLS point clouds

2.2 Study area

Copou Park, also known as Copou Gardens, is the oldest public park in Iași, Romania. Its development began in 1834, during the reign of Prince Mihail Sturdza, making it one of the earliest public gardens in Romania and a historic landmark of Iași. At the centre of the park stands the Lions' Obelisk (erected in 1834), a 13.5 m tall monument. Other notable landmarks within the park include Eminescu's Linden Tree, the Mihai Eminescu Museum, and Junimea Alley. Today, Copou Park remains a popular destination for both locals and visitors, hosting poetry festivals, photography exhibitions, and arts and crafts fairs.

Spanning 0.7 ha, the study area is characterized by diverse tree species, namely linden, maple, fir and thuja (Figure 2).

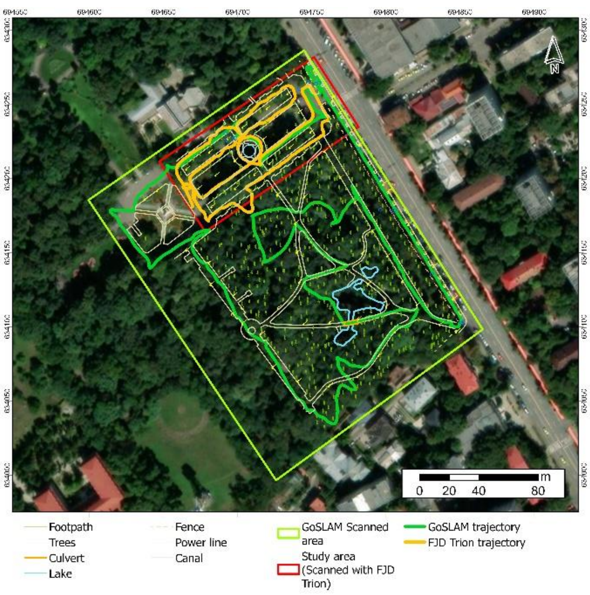

Figure 2: The Copou Park (light green) and the study area (red) located in Iasi, Romania

2.3 Data Acquisition Using GoSlam RS100i and the FJD Trion S1 HMLS equipment

Both, the GoSLAM RS 100i and the FJD Trion S1, are lightweight, handheld mobile LiDAR scanner leveraging SLAM (Simultaneous Localization and Mapping) to perform real-time localization and 3D mapping without exclusive reliance on GNSS. Using the GoSLAM RS 100i scanner (Figure 3 a), the "Copou Park" (Figure 2 – light green rectangle) was scanned in approximately 20 minutes following one walking path of 1455 m in April 2025. In order to carry out data acquisition, the FJD Trion S1 mobile LiDAR system was configured in backpack mode and integrated with a GNSS receiver for accurate georeferencing (Figure 3 b,c). The study area was scanned in September 2025, following a different walking trajectory of 667 m restricted to the area of interest (Figure 2 - red rectangle), with a total acquisition time of approximately 7 minutes.

(a) (b) (c)
Figure 3: Data acquisition using the GoSLAM mobile Scanner (a) and FJD Trion S1 (b), (c).

Table 1 presents the technical specifications of the GoSLAM RS100i and FJD Trion S1 sensors, as reported in the respective manufacturer documentation.

Sensor	GoSLAM RS100i	FJD Trion S1
Field of View (FOV)	360° × 285°	360° × 270°
Number of laser lines	16	16
Scanning speed	320,000 points/s	320,000 points/s
Scanning distance	120 m	120 m
Accuracy	up to ~1 cm	~2 cm (relative)

Table 1: Technical specifications of the GoSLAM RS100i and FJD Trion S1 sensors, based on manufacturer-provided technical documentation

2.4 Marking and measuring the GCPs

Prior to data acquisition, 26 ground control points (GCPs) were uniformly distributed across the park and materialized using metallic bolts and wooden stakes within the vegetated areas. The position of each GCP was measured using GNSS RTK technology, with a two-minute observation interval, employing a multi-band Geomax Zenith60 receiver that provides centimetric accuracy through the Romanian Positioning Determination System (ROMPOS). The planimetric coordinates of the GCPs were referenced to the Romanian national coordinate system Stereographic 1970 (STEREO-70), while ellipsoidal heights were converted from the ETRS89 European datum to Black Sea 1975 normal heights, consistent with the RO Const/NH vertical datum.

To ensure visibility within the HMLS point cloud, each GCP was marked with a plexiglass target plate featuring a high-contrast pattern composed of two black and orange triangles (Figure 4).

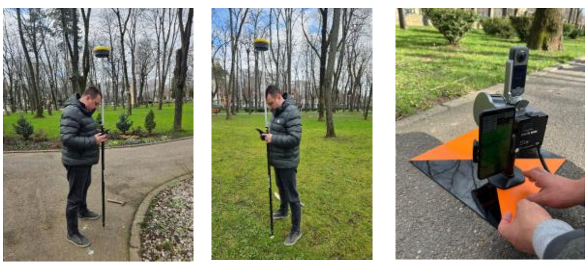

(a) (b) (c)
Figure 4: Marking and measuring the GCPs on the field: metallic bold (a), wooden stick (b), plexiglass plate (c).

2.5 Reference data acquisition for DBH estimation

The measurement of diameters is carried out with the standardized forest caliper, generally consisting of a graduated ruler and two perpendicular arms on it, one of which is movable, and the other is fixed (Figure 5). To ensure that the measurement operation can be carried out under appropriate conditions in terms of precision, the following rules must be applied (www.aces.edu):

- Use of forest calipers in perfect technical condition, with arms parallel and perpendicular to the graduated ruler, which is periodically checked even during the same working day, any deviations being corrected;
- Strict adherence to the measuring height (1.30 m from the ground);
- Placement of the caliper perpendicular to the axis of the tree, so that three points of contact of the caliper with the tree are at the same level, and the reading is taken while the instrument is fixed on the tree;
- Cleaning the measuring site from lichens and mosses, without affecting the bark of the tree being measured;
- For trees with irregular cross-sections, two perpendicular diameters are measured, and then the arithmetic mean of those two readings is recorded;
- The rounding of the measured diameters must be done with great care, avoiding the introduction of systematic errors.

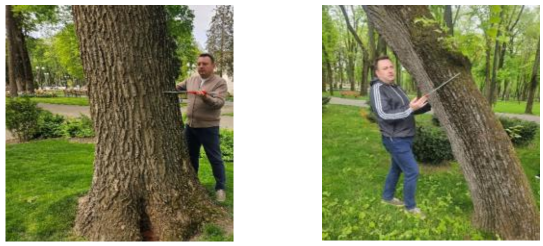

(a) (b)
Figure 5: Measuring DBH in the field using a forest caliper: straight trunk (a) and inclined trunk (b)

A total of 69 trees within the study area were measured and classified into two DBH classes (Table 2). Most trees have a DBH between 25 and 55 cm, with only one tree exceeding 1 m in diameter (i.e 1.08 m) (Figure 6).

DBH interval [cm]	20<DBH<40	DBH>40
Number of trees	32	37

Table 2: Number of tree DBH in two classes.

Due to the time difference between acquisitions using the two scanning systems, six trees were cut down, resulting in 63 reference trees for the FJD Trion HMLS point cloud.

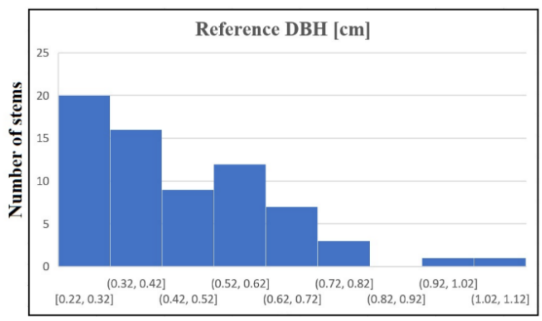

Figure 6: DBH distribution of the 69 trees as measured in the field (bin width is 10 cm).

https://doi.org/10.5194/isprs-archives-XLIX-B1-2026-33-2026

2.6 Reference data acquisition for tree position

All three positions were measured using a robotic total station i.e Geomax Zoom 95 (Figure 7 a) and prism setup in standard mode (Figure 7 b) with a precision of 1 mm according to the manufacturer's technical specifications.

(a) (b)

Figure 7: Tree position measurement using the GeoMax Zoom 95 robotic total station (a) and the prism (b)

2.7 High-Resolution Mobile Laser Scanning (HMLS) point clouds registration and georeferencing

In the case of the GoSLAM hand-held laser scanner, the registration process was performed automatically with the Simultaneous Localization and Mapping (SLAM) algorithm implemented GoSLAM Mapping Master software. The registered point cloud is given in a local coordinate system, with origin at the start/end position of the walking path. To determine the precise locations of the GCPs, manual measurements were conducted directly within the point cloud using CloudCompare software. The intersections of the triangles were identified and measured manually. Of the total GCPs, five were used for indirect georeferencing of the HMLS point cloud through a Helmert transformation, and the remaining 21 served as Check Points (ChPs) to evaluate the accuracy of the indirect georeferencing process (Oniga et al., 2024). The achieved georeferencing accuracy, assessed using the ChPs, resulted in root mean square errors of $RMSE_X$ = 3.1 cm, $RMSE_Y$ = 2.5 cm, and RMSE_z = 2.3 cm.

For FJD Trion S1 the system trajectory was processed using the FJD Trion Model software, which integrates the onboard inertial measurements with real-time kinematic (RTK) positioning. The RTK corrections were used to refine the global georeferencing of the trajectory. The resulting direct georeferencing accuracy was assessed based on 6 ChPs, yielding results comparable to those obtained with the GoSLAM scanner.

2.8 Point cloud filtering and subsampling

To reduce high-frequency noise in the HMLS point cloud, a local plane-based denoising approach was applied using the *Noise Filter* function in CloudCompare. A neighborhood of the 25 nearest neighbours was used to estimate local surface geometry, and points whose deviation from the fitted plane exceeded a relative error threshold of 1.8 (deviations greater than 1.8 times the local surface variation) were removed. This threshold was determined empirically to account for the heterogeneous characteristics of the urban park environment. Given the presence of both smooth artificial surfaces and naturally irregular features such as grass, soil and shrubs, a moderate threshold was selected to suppress isolated high-frequency noise while preserving meaningful geometric variation. In addition, isolated points with fewer than three neighbours were removed to eliminate spurious single returns. The filtering parameters were refined through iterative testing and visual assessment to ensure effective noise reduction without compromising essential structural details. Subsequently, subsampling was performed using the *Subsampling* function in CloudCompare, applying the *Spatial* method with a defined minimum distance between points. The number of points at each processing stage, including filtering and subsampling, for both the GoSLAM RS100i and FJD Trion S1 datasets is summarized in Table 3. A significant reduction in point density can be observed after subsampling, particularly for coarser resolutions. A coarser subsampling resolution of 4 cm leads to a significant decrease in point density relative to 2 cm, reducing the number of points by approximately 45% for the GoSLAM RS100i and over 60% for the FJD Trion S1.

Point cloud	GoSLAM RS100i	FJD Trion S1
Original point cloud	24.174.207	227.986.732
Filtered point cloud	23.195.897	214.353.186
Subsampled at 2 cm	11.923.249	42.301.376
Subsampled at 3 cm	8.665.183	24.680.730
Subsampled at 4 cm	6.616.789	15.945.040

Table 3: Point cloud size at different processing stages and subsampling resolutions

The filtered and subsampled point clouds at 2 cm resolution for both datasets are presented in Figure 8, illustrating a single tree.

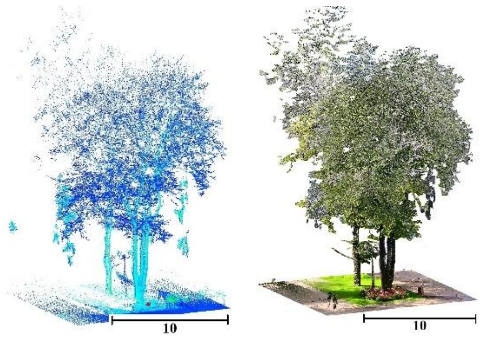

(c) (d)

Figure 8: Filtered and subsampled at 2 cm space distance GoSLAM point cloud of a single tree (a) and FJD Trion S1 point cloud of the same tree (b)

2.9 Digital Terrain Model (DTM), Digital Surface Model (DSM), and normalized Digital Surface Model (nDSM)

The Digital Terrain Model (DTM) was generated using the OPALS software through a hierarchical and iterative filtering approach designed to progressively refine the ground surface representation. The workflow reduces the number of points by selecting representative ground candidates and iteratively refining the terrain surface from coarse to fine spatial resolution. To reduce the point density and retain only potential ground points, a thinning procedure was applied. The lowest last echo within raster cells of 0.1 m was selected as the basis for the initial terrain estimation. A coarse representation of the terrain was generated by aggregating the thinned dataset into larger raster cells (5 m resolution) and extracting the 5th percentile of elevation values, which serves as an approximation of the ground surface. The terrain surface was interpolated using Delaunay triangulation and gaps were filled using triangulation-based interpolation. Subsequently, an iterative refinement procedure was applied using progressively finer grid resolutions (0.5 m, 0.25 m, and 0.1 m). At each iteration, points were filtered based on their normalized height relative to the terrain surface, ensuring that only ground candidates were used for interpolation. The final terrain model was generated using the moving planes interpolation method and visually assessed using a hillshade representation (Figure 9 a). The derived DTM was used to normalize the heights of all points. The derived normalizedZ is available as an additional attribute.

After the generation of the DTM, the DSM was produced with the OpalsDSM module using a combined approach based on the highest point within 0.25 m cells and grid-based interpolation approach for cells where no points were available or for smooth surfaces. For the grid-based approach, the surface elevation was estimated for each grid cell using the 20 nearest points located within a search radius of <3 m (Figure 9 b). To minimize the influence of points that do not lie on the canopy surface, only the highest points within 0.125 m cells are used to find the 20 nearest neighbors. Further details can be found in Hollaus et al. (2010).

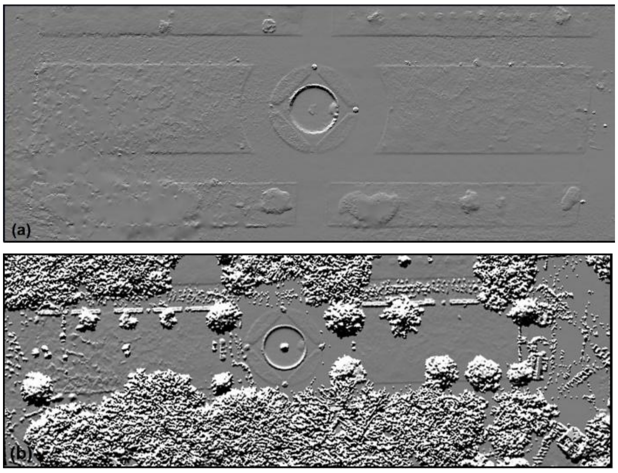

Figure 9: Hillshades of (a) the Digital Terrain Model (DTM) and (b) the Digital Surface Model (DSM) of the study area, obtained based on the GoSLAM point cloud

To derive canopy heights, a normalized Digital Surface Model (nDSM) was computed by subtracting the terrain elevation from the DSM using the *opalsAlgebra* module. Points exceeding a normalized height threshold of 60 m were excluded to remove potential outliers and noise and only positive height differences were retained.

2.10 Stem point extraction

To identify potential stem points, the normalized point cloud was filtered based on the height above ground (normalizedZ). Only points located between 1 m and 3 m above the terrain surface were selected, as this height interval typically corresponds to the lower stem section while excluding most branches and canopy elements. In this height layer also points from e.g. bushes and branches are available. Next, the processing workflow aimed to isolate points corresponding to vertically oriented stem structures through a sequence of neighbourhood-based statistical analysis and geometric filtering.

Initially, some descriptors characterizing local point density and vertical structure were calculated. So, local point-cloud statistics were computed for each point using a two-dimensional neighbourhood with a radius of 0.2 m. The derived attributes included the number of neighbouring points, the local point-distance measure and the 10^{th} and 90^{th} percentiles of the vertical coordinate distribution. These descriptors characterize local point density and vertical structure and form the basis for subsequent filtering.

A first filtering step retained only points with low local vertical-distance variability (dZPdist < 0.05), thereby removing points with irregular neighbourhood configurations and preserving candidates with more homogeneous local geometry.

Subsequently, an iterative normal-based filtering procedure was applied. Surface normals were estimated using a three-dimensional neighbourhood with a radius of 0.05 m and a maximum of 1000 neighbouring points. The computation also stored extended meta-information describing the local geometric structure. In the case of vertically oriented objects such as tree stems, the normal vectors are expected to lie predominantly in the horizontal plane. Therefore, the vertical component of the normal vector (NormalZ) was used as an indicator of surface orientation. Points with NormalZ < 0.2 were retained, as the vertical component is close to zero for stem surfaces. This normal estimation and filtering step was repeated three times in succession to progressively eliminate non-vertical elements and refine the set of stem candidates.

Following the geometric filtering, additional attributes were derived to increase the discrimination of stem-like structures. A compactness indicator (Rpc_pdis) was defined as the normalized difference between the local point count and the point-distance measure, reflecting the degree of local point clustering. Furthermore, the vertical range of the neighbourhood was quantified as the difference between the 90^{th} and 10^{th} height percentiles, representing the vertical extent of the local point distribution. An additional ratio was computed to relate point density to vertical spread.

In the final selection step, points were classified as stem candidates if they simultaneously exhibited a very high compactness response (Rpc_pdis > 0.99995) and a minimum vertical extent of 0.5 m, so points corresponding to geometrically coherent, vertically elongated and densely sampled structures.

For deriving the final stem position a segmentation (i.e. region growing) of the candidate stem was done, whereas a neighbourhood search radius of 0.2 m and a minimum point threshold of 20 was applied. The stem position is defined with the centroid of the minimum bounding x-y rectangle of the derived segment. Furthermore, the radius of the stem is approximated based on the minimum bounding rectangle.

2.11 DBH estimation

To initialise stem modelling, the detected stem positions were supplement with approximation parameters required for subsequent DBH estimation. For each stem position, the local terrain elevation was determined as the maximum DTM elevation within a radius of 0.4 m. Based on this local terrain height, a vertical fitting interval was defined around breast height by setting lower and upper bounds to $z_{DTM} + 1.1$ m and $z_{DTM} + 1.5$ m, respectively. In addition, an initial stem radius estimate was derived from the previous section segmentation (see 2.8). The resulting parameters (local DTM height, fitting height interval, and radius estimate) were stored as attributes in the OPALS dataset and used to construct the approximation input for cylindrical stem fitting.
For each detected stem position, tree height was estimated by computing the maximum elevation of neighbouring DSM points within a 1.5 m radius and subtracting the local ground elevation at the stem position.

$$H = z_{max} - z_{DTM,stem} \quad (1)$$

The resulting height estimate and the stem coordinates were stored as attributes and exported to an approximation file providing initial parameters for DBH modelling. Based on these approximations, the *opalsDBH* module was employed to estimate the DBH using the cylindrical (*-geometryModel cylinder*) fitting models within a defined vertical interval around breast height. To improve robustness, the procedure was performed iteratively. After an initial fitting pass, the estimated stem centres were spatially consolidated by neighbourhood averaging and grid-based thinning to remove duplicate or unstable detections. Subsequently, the point cloud was linked to the refined stem centres and the radial distribution of points around each centre was analysed using distance-based statistics (point counts, quantiles, and standard deviation). Stems failing geometric consistency criteria (e.g., excessive offsets or high radial dispersion) were rejected. A refined approximation file was then generated and a second DBH fitting iteration was performed, resulting in the final DBH estimates.

3. RESULTS AND DISCUSSION

Detected stems were matched to those recorded in the field inventory, and a detection was considered correct if its position was located within a distance of 0.5 m from a reference stem. Such detections were classified as true positives (TP). To assess the performance of the autonomous stem detection, precision and recall were computed as follows (Bruggisser et al., 2020):

$$precision = \frac{TP}{TP + FP} \tag{2}$$

$$recall = \frac{TP}{TP + FN} \tag{3}$$

where false positives (FP) represent segments in the point cloud incorrectly identified as stems by the algorithm but not present in the field inventory, and false negatives (FN) correspond to stems recorded in the field inventory that were not detected in the point cloud (Table 3).

The number of estimated DBH values successfully matched to the field inventory was quantified. The accuracy of the estimates was subsequently assessed in terms of bias and root mean square error (RMSE) (Bruggisser et al., 2019):

$$bias = \frac{1}{n}\sum_{i=1}^{n}(DBH_{estim,i} - DBH_{ref,i}) \tag{4}$$

$$RMSE = \sqrt{\frac{\sum_{i=1}^{n}(DBH_{estim,i} - DBH_{ref,i})^2}{n}} \tag{5}$$

where $DBH_{estim,i}$ corresponds to the i-th DBH estimated from the point cloud, $DBH_{ref,i}$ refers to the respective measurement obtained from the field inventory, and n denotes the number of matched DBHs field (Table 4).

The number of correctly detected trees varied between the two systems and across subsampling spacings. For the GoSLAM RS100i system, the number of correctly detected trees decreased from 67 at 2 cm spacing to 63 at 3 cm and further to 37 at 4 cm, out of a total of 69 trees. The result obtained at 2 cm spacing is consistent with the findings of Liu et al. (2021) where 56 out of 58 trees in an urban forest environment were correctly identified using a Velodyne VLP-16 LiDAR sensor in winter condition. In contrast, the FJD Trion S1 system showed more stable performance, with 54, 55, and 55 correctly detected trees at 2 cm, 3 cm, and 4 cm spacing, respectively, out of a total of 63 trees. This difference can be attributed to variations in point cloud density, as the GoSLAM RS100i data at each sampling distance, contain approximately three times fewer points than the FJD Trion S1 system. Furthermore, for GoSLAM RS100i, increasing the spacing resulted in a reduction in both detected and correctly detected trees, as well as a marked decrease in recall (from 97.1% at 2 cm to 53.6% at 4 cm). This suggests a strong dependence on point density. In contrast, the FJD Trion S1 was less sensitive to subsampling, maintaining relatively stable recall values (~86–87%) across all spacings. This indicates greater robustness to reduced point density. The results are based on the second iteration of the workflow, with only minor differences from the first. In the GoSLAM dataset, two trees were not re-detected, while in the FJD Trion dataset, differences of 4–7 trees were observed across subsampling levels. When tree positions are known a priori, a single iteration is sufficient and false positives can be reduced by matching detections to reference locations.

	GoSLAM RS100i			**FJD Trion S1**		
Space between points [cm]	2	3	4	2	3	4
Detected trees	106	79	58	86	86	69
Correctly detected trees	67	63	37	54	55	55
Precision [%]	63.2	79.7	63.8	62.8	64.0	79.7
Recall [%]	97.1	91.3	53.6	85.7	87.3	87.3
DBH bias (error < 8 cm) [cm]	2.4	2.5	2.1	1.7	1.7	2.1
DBH RMSE for all trees [cm]	4.1	3.8	3.5	4.6	4.5	4.9
DBH RMSE (error < 8 cm) [cm]	3.6	3.5	3.5	3.4	3.3	3.5

Table 4: DBH estimation performance of the GoSLAM RS100i and FJD Trion S1 mobile LiDAR systems under different point spacings

The two systems exhibited distinct detection characteristics. The GoSLAM RS100i achieved very high recall, particularly at 2 cm (97.1%) and 3 cm (91.3%), indicating that most reference trees were successfully detected. Notably, the recall at 2 cm slightly better than the value reported by Liu et al. (2021) i.e 96.6%. However, this was accompanied by lower precision values (63.2–79.7%), suggesting a higher number of false positives. In contrast, the FJD Trion S1 showed a more balanced performance, with recall values ranging from 85.7% to 87.3% and precision between 62.8% and 79.7%. Notably, precision increased at 4 cm spacing (79.7%), indicating improved robustness against false detections at coarser resolutions. Some undetected trees can be attributed to incomplete stem representation, where less than half of the trunk circumference was captured due to limitations in the scanner trajectory. As reported by Bruggisser et al. (2020), a minimum stem coverage of approximately 50% is required for reliable tree detection and DBH estimation. In addition, missed detections may also occur due to residual noise points in the vicinity of the tree trunk, which can interfere with the segmentation process. This effect was observed primarily in the FJD Trion S1 dataset, as the acquisition was performed under leaf-on conditions, leading to increased vegetation-induced noise around the stems (Figure 10 a).

The comparison between DBH estimates derived from the GoSLAM RS100i and FJD Trion S1 systems revealed consistent performance across all subsampling spacings (2–4 cm). Both systems exhibited a systematic positive bias, indicating a general tendency to overestimate DBH relative to the reference dataset. The bias ranged from 1.68 to 2.10 cm for FJD Trion S1 and from 2.14 to 2.54 cm for GoSLAM RS100i, with GoSLAM consistently showing slightly higher bias values. In terms of accuracy, the mean absolute error (MAE) varied between 2.79–3.06 cm for FJD Trion S1 and 3.00–3.04 cm for GoSLAM RS100i, while the RMSE values were comparable for both systems, ranging from approximately 3.30 to 3.55 cm. The proposed workflow for DBH estimation achieves an accuracy comparable to state-of-the-art methods, with RMSE values ranging between 3.3 cm and 3.6 cm. Similarly, Liu et al. reported an RMSE of 3.31 cm in a natural forest plot and of 1.98 cm in an urban plot. The observed DBH discrepancies can also be linked to acquisition geometry and terrain modeling uncertainties, as DBH is measured at 1.3 m above ground level (Figure 10 b). In addition, pronounced DBH differences (>8 cm) were associated with trees exhibiting irregular stem morphology and also vegetation cover of the tree trunk (Figure 10 b,c).

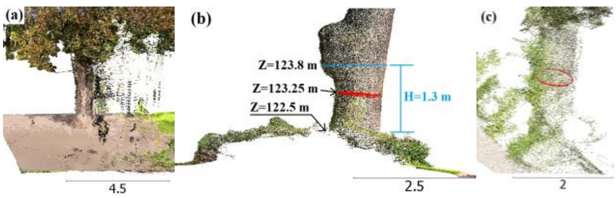

Figure 10: Examples of error sources in the FJD Trion dataset: (a) undetected tree due to residual noise around the trunk; (b) tree with a high DBH error (RMSE = 14.6 cm) caused by an irregular stem shape and DTM inaccuracies; and (c) tree with a high DBH error (RMSE = 8.2 cm) caused by vegetation cover.

Overall, the FJD Trion S1 demonstrated slightly lower bias and marginally better accuracy, although the differences between the two systems were relatively small. The influence of subsampling spacing (2 cm, 3 cm, and 4 cm) on DBH estimation accuracy was limited. For both systems, only minor variations in bias and error metrics were observed across spacings. Statistical testing confirmed that subsampling spacing did not have a significant effect on DBH estimation for either system (FJD Trion S1: $p = 0.73$; GoSLAM RS100i: $p = 0.76$). This indicates that increasing the subsampling spacing up to 4 cm does not significantly degrade DBH estimation accuracy, suggesting robustness of both methods to point cloud density reduction.

The distribution of absolute DBH errors further supports these findings, showing similar interquartile ranges and median values across all subsampling spacings (Figure 11). This indicates that increasing the subsampling spacing up to 4 cm does not significantly degrade DBH estimation accuracy, highlighting the robustness of both methods to point cloud density reduction.

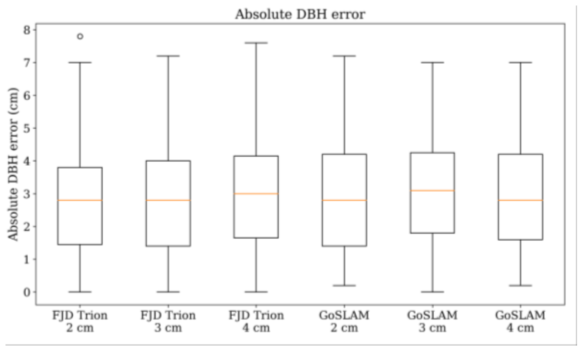

Figure 11: Boxplot of absolute DBH estimation errors for GoSLAM RS100i and FJD Trion S1 across subsampling spacings (2 cm, 3 cm, and 4 cm)

The histograms of DBH differences showed that error distributions for both systems were generally centered close to zero, with a slight shift toward positive values, confirming the observed overestimation bias (Figure 12). A weak negative correlation between DBH error and tree size was observed, particularly for the GoSLAM RS100i system (up to $r = -0.28$, $p < 0.05$). The results indicate a weak negative trend, with smaller trees exhibiting a larger spread of errors, while larger trees show more stable and generally lower deviations. For the FJD Trion S1 system, the relationship was not statistically significant (Figure 13).

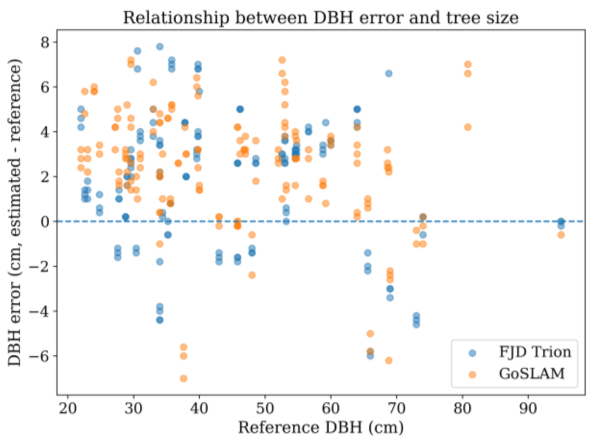

Figure 13: Relationship between DBH estimation error and reference DBH for GoSLAM RS100i and FJD Trion S1. The dashed line indicates zero error.

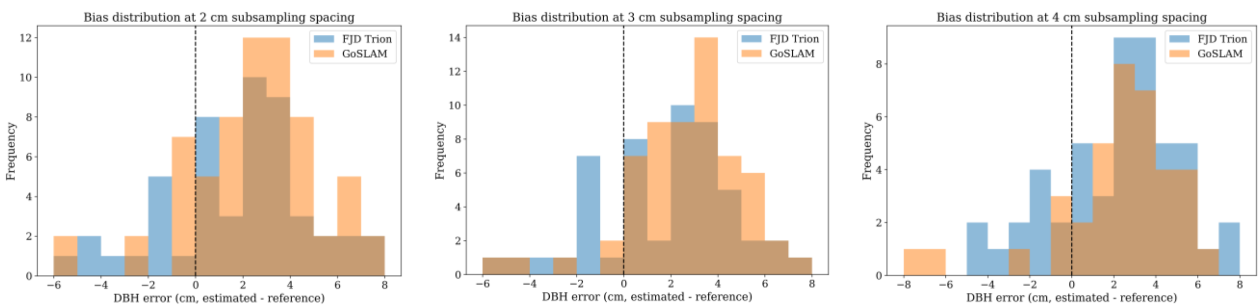

(a) (b) (c)

Figure 12: Relative histograms of differences between DBH estimates derived from the GoSLAM RS100i and FJD Trion S1 systems and the reference dataset for subsampling spacings of 2 cm (a), 3 cm (b), and 4 cm (c). Bin widths are set to 1 cm, differences are measured in [cm]. Orange: GoSLAM, blue: FJD Trion, brown: overlay of the histograms.

4. CONCLUSIONS

This study presented an integrated workflow for automatic tree detection and diameter at breast height (DBH) estimation from handheld mobile laser scanning (HMLS) data, and evaluates its performance using the GoSLAM RS100i and FJD Trion S1 systems in an urban park environment. The results indicate that tree detection performance is strongly influenced by point cloud density and acquisition conditions. While the FJD Trion S1 dataset showed generally stable detection results, its detection rate was affected by the presence of vegetation, as the data were acquired in September under leaf-on conditions, compared to April (leaf-off) for the GoSLAM dataset. In contrast, for the GoSLAM data at 2 cm spacing, almost all trees were correctly detected including inclined stems, except for two cases. DBH estimation proved to be relatively robust, with comparable accuracy across different subsampling resolutions and between the two systems, despite a small systematic bias. Overall, the proposed workflow demonstrates that HMLS data can provide reliable DBH estimates for urban tree inventory applications, while emphasizing the importance of acquisition conditions and data quality. Future work should focus on improving detection robustness in the presence of undergrowth vegetation and noise, as well as under lower point density conditions.

References

Binot, J.-M., Pothier, D., Lebel, J., 1995. Comparison of relative accuracy and time requirement between the caliper, the diameter tape and an electronic tree measuring fork. *Int. Arch. Photogramm. Remote Sens. Spatial Inf. Sci.*, 71 (2), 197–200. https://doi.org/10.5558/tfc71197-2

Bruggisser, M., Hollaus, M., Kükenbrink ,D., Pfeifer, N., 2019. Comparison of forest structure metrics derived from uav lidar and als data, ISPRS Ann. Photogramm. Remote Sens. Spat. Inf. Sci., IV-2/W5, pp. 325-332, 10.5194/isprs-annals-IV-2-W5-325-2019

Bruggisser, M, Hollaus, M., Otepka, J., Pfeifer, N., 2020. Influence of ULS acquisition characteristics on tree stem parameter estimation, ISPRS Journal of Photogrammetry and Remote Sensing, Volume 168, pp. 28-40, ISSN 0924-2716, 10.1016/j.isprsjprs.2020.08.002

Fan, W., Liu, H., Xu, Y., Lin, W., 2021. Comparison of estimation algorithms for individual tree diameter at breast height based on hand-held mobile laser scanning. Scand. J. For. Res. 2021, 36, 460–473.

Gillner, S., Vogt, J., Tharang, A., Dettmann, S., Roloff, A., 2015. Role of street trees in mitigating effects of heat and drought at highly sealed urban sites. *Landsc. Urban Plan.*, 143, 33–42. https://doi.org/10.1016/j.landurbplan.2015.06.005

He, S., Osman, Z., Cladera, F., Ong, D., Rai, N., Green, P.C., Kumar, V., Chaudhari, P., 2025. Estimating the diameter at breast height of trees in a forest with a single 360° camera. In: *Proc. IEEE ICRA Workshop on Novel Approaches for Precision Agriculture and Forestry with Autonomous Robots*, 2025.

Hollaus, M, Mandlburger, G, Pfeifer, N, Mücke, W., 2010. Land cover dependent derivation of digital surface models from Airborne laser Scanning data. In IAPRS Volume XXXVIII Part 3A, pp. 221–226. http://hdl.handle.net/20.500.12708/42587

Jayasooriya, V.M., Ng, A.W.M., Muthukumaran, S., Perera, B.J.C., 2017. Green infrastructure practices for improvement of urban air quality. *Urban For. Urban Green.*, 21, 34–47. https://doi.org/10.1016/j.ufug.2016.11.007

Koreň, M., Mokroš, M., Bucha, T., 2017. Accuracy of tree diameter estimation from terrestrial laser scanning by circle-fitting methods. *Int. Arch. Photogramm. Remote Sens. Spatial Inf. Sci.*, XLII-2/W4, 122–128. https://doi.org/10.1016/j.jag.2017.07.015

Liang, X., Kankare, V., Hyyppä, J., Wang, Y., Kukko, A., Haggrén, H., Yu, X., Kaartinen, H., Jaakkola, A., Guan, F., Holopainen, M., Vastaranta, M., 2016. Terrestrial laser scanning in forest inventories. ISPRS J. Photogramm. Remote Sens. 115, 63–77. http://dx.doi.org/10.1016/j.isprsjprs.2016.01.006

Liang, X., Kankare, V., Hyyppä, J., Yu, X., Kaartinen, H., Vastaranta, M., Holopainen, M., Wang, Y., Kukko, A., Haggrén, H., Jaakkola, A., Guan, F., 2018. Feasibility of terrestrial laser scanning for collecting stem volume information from single trees. ISPRS J. Photogramm. Remote Sens. 135, 44–55.

Liu, L., Zhang, A., Xiao, S., Hu, S., He, N., Pang, H., Zhang, X., Yang, S., 2021. Single tree segmentation and diameter at breast height estimation with mobile LiDAR. *IEEE Access*, 9, 24314–24325. https://doi.org/10.1109/ACCESS.2021.3056877

Liu, N., Zhang, F., 2025. Urban green spaces and flood disaster management: toward sustainable urban design. *Front. Public Health*, 13, Article 1583978. https://doi.org/10.3389/fpubh.2025.1583978

Mandlburger, G., Hollaus, M., Glira, P., Wieser, M., Milenković, M., 2015. First examples from the riegl vux-sys for forestry applications. In: Proceedings of SilviLaser. 28-30 September 2015, La Grande Motte, France. pp. 105–107

Oniga, E., Boroianu, B., Morelli, L., Remondino, F., and Macovei, M.: Beyond ground control points: cost-effective 3D building reconstruction through GNSS-integrated photogrammetry, Int. Arch. Photogramm. Remote Sens. Spatial Inf. Sci., XLVIII-2/W4-2024, 333–339, https://doi.org/10.5194/isprs-archives-XLVIII-2-W4-2024-333-2024.

Oveland, I., Hauglin, M., Gobakken, T., Næsset, E., Maalen-Johansen, I., 2017. Automatic estimation of tree position and stem diameter using a moving terrestrial laser scanner. *Int. Arch. Photogramm. Remote Sens. Spatial Inf. Sci.*, XLII-2/W4, 350. https://doi.org/10.3390/rs9040350

Pfeifer, N., Mandlburger, G., Otepka, J., Karel, W., 2014. OPALS–A framework for Airborne Laser Scanning data analysis. Computers, Environment and Urban Systems, 45, 125–136.

Piermattei, L., Karel, W., Wang, D., Wieser, M., Mokroš, M., Surovy, P., Koreň, M., ` Tomaštík, J., Pfeifer, N., Hollaus, M., 2019. Terrestrial structure from motion photogrammetry for deriving forest inventory data. Remote Sens. 11 (8), 950. http://dx.doi.org/10.3390/rs11080950

Zhou, S., Kang, F., Li, W., Kan, J., Zheng, Y., He, G., 2019. Extracting Diameter at Breast Height with a Handheld Mobile LiDAR System in an Outdoor Environment. *Sensors* 2019, *19*, 3212. https://doi.org/10.3390/s19143212

https://www.aces.edu/wp-content/uploads/2022/02/Chapter-7_FOR-2082_022422L-G.pdf